Chapter 2
An objective method to associate local weather extremes with characteristic circulation stuctures

Corinna Ziemer [1] Katarzyna Marczyska [2] Anna Szczepańska [2] Joanna Zyprych [2] Jos Hageman [3] Timo Doeswijk [3†]

Abstract:
In this paper we give methods to find characteristic circulation patterns which are connected to local extreme temperature anomalies. Two data reduction techniques are applied: Legendre polynomial fitting and watershedding. For polynomial fitting a clear trend is found with respect to local temperatures. However, the trend is not distinctive enough to give clear answers on the type of circulation patterns belonging to local extremes. The main advantage of watershedding is that the physical properties of the circulation patterns are retained while the dimension of the data is largely reduced. Expert knowledge, however, is needed to model these main features as predictors.
KEYWORDS: *circulation pattern, extreme temperature, watershedding, Legendre polynomial.*

[1]Centre for Industrial Mathematics, University of Bremen, Germany
[2]Poznan University of Life Sciencies, Poland
[3]Biometris, Wageningen University, The Netherlands
[†]corresponding author: `timo.doeswijk@wur.nl`

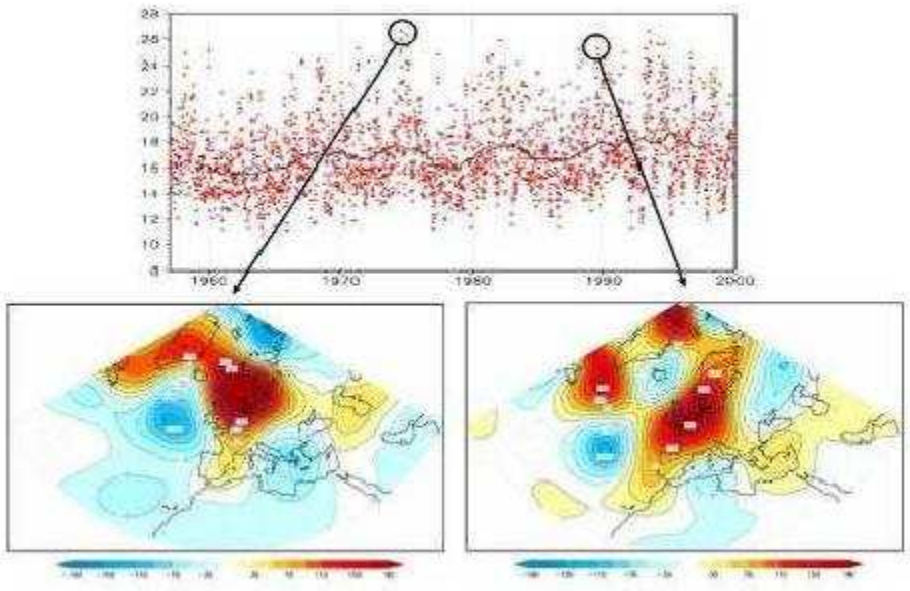

Figure 2.1: Upper panel: time series of maximum daily temperatures of the months july and august in the years 1958-2000; left panel - circulation pattern that relates to a local extreme temperature in 1975; right panel - circulation pattern that relates to a local extreme temperature in 1983

2.1 Introduction

Meteorological events such as severe storms, heavy rains, cold surges or drought which occur locally are usually connected to circulation structures of much larger scale in the atmosphere. In this paper we study the relation between local extreme temperatures and circulation patterns in the atmosphere. In meteorology it can be observed that extreme temperatures (temperature anomalies) appear for several different states of atmosphere circulation. For example, in 1975 a high pressure anomaly was located above Scandinavia leading to advection of warm, dry, continental air into the Netherlands by easterly winds and local extreme heat. Eight years later, a high pressure anomaly was located right above the Netherlands with clear skies, no wind, an abundance of sunshine and as a result, extreme high temperatures. Figure 2.1 shows these two different circulation patterns which caused local temperature extremes.

The concept of weather regimes was considered by Michelangeli et al. [1]. The authors compared two different definitions of weather regimes. The first definition treats weather

regimes as the states of the atmosphere with the highest probability of occurrence. In the second case weather regimes are defined as the states for which large-scale motion is stationary in the statistical sense. The authors applied these methods on the same dataset and they showed that these methods give the same number of weather regimes - four over the Atlantic sector and three over the Pacific sector. They observed that the patterns differ significantly and the investigation of the tendency, or drift, of clusters shows that recurrent flows have a systematic slow evolution, explaining this difference. The patterns are in agreement with the one obtained from previous studies, but their number differ. Panja and Selten [2] presented a new method to optimally link local weather extremes to large scale atmospheric circulation structures. This method objectively identifies, in a robust manner, the different circulation patterns that favor the occurrence of local weather extremes and is based on considering linear combinations of the dominant Empirical Orthogonal Functions that maximize a suitable statistical quantity. Moreover, Salameh and Dobrinski [3] related the occurrence of extreme events (in terms of temperature, precipitation and wind speed) to weather regimes. They evaluated the uncertainty associated with North Atlantic weather regime clustering with the re-analyses data set and its impact on the relationship between weather regimes and extreme events over and around the North Atlantic.

The aim of this paper is to find a method that identifies pressure patterns which lead to extreme values of temperature in one fixed point and to work out a method to predict when local temperature extremes occur.

To analyze circulation patterns in relation to extreme temperature anomalies we use date obtained from the ERA-40 reanalysis dataset. The data of the circulation patterns contained the pressure field for 1372 grid points which are arranged on 20^0 N - 90^0 N latitude and 60^0 W - 60^0 E longitude ($2.5^0 \times 2.5^0$ latitude-longitude grid). A time series of daily circulation patterns were available for July and August of the years 1958-2000 (all together 43 years and 2666 time points in total). The local temperature was taken at the center of the Netherlands (52.5^oN, 5^oE). The 5 per cent most extreme (positive) anomalies were taken as extreme values. In this way 133 circulation patterns were connected to local extreme temperatures. One of the main issues to be dealt with is data reduction. Two methods are used and explored: 1) Legendre polynomial fitting and 2) watershedding.

2.2 Modelling approaches

The discrete pressure field contains $28 \times 49 = 1372$ data points. Using this raw data as an input, the model would have to base its decision (whether the pattern belonged to an extreme temperature) on a huge amount of data. Directly using these data causes prob-

lems such as ill-conditioned matrices because of high correlations between grid points and long computation times. Therefore, first the available data is reduced while retaining the information before processing it. That can be achieved by fitting Legendre polynomials to the pressure distribution or by the watershedding technique. As a second step, a connection between the global weather situation and temperature has to be found. In this work, the method of linking the pressure anomaly patterns with the local temperature extremes uses empirical data. In order to see whether the method gives correct results, firstly the patterns belonging to the most extreme temperatures are picked out from the empirical data. Then this set is split into reference patterns (used for calibrating the method) and validation patterns (used to check whether the method works correctly).

2.2.1 Data Reduction

We have 133 patterns with extreme temperature in one fixed point. Each circulation pattern can be described as 28×49 pressure table where rows represents latitude and columns longitude. Mathematically speaking, we are looking for a function from the set of pressure patterns $\{Z(t_i)\}$ to a set of characteristic parameters $\{C(t_i)\}$, where t_i indicates the point in time at which the pressure measurement was taken. When choosing the dimension of the space of characteristic parameters much smaller than the dimension of the patterns' space, we can store approximately the same amount of information with much less data.

Legendre Polynomials

The general idea in this approach is a known result from Linear Algebra: a function f belonging to a finite dimensional space of functions X_N (e.g. all polynomials of order N) can be represented by a linear combination of basis functions $P_l \in X_N,\ l = 1, \ldots, N,\ \ N \in \mathbb{N}$:

$$f(x) = \sum_{l=1}^{N} \alpha_l P_l(x) \qquad \forall x \in \mathrm{Dom}(f) \tag{2.1}$$

where $\mathrm{Dom}(f)$ denotes the domain of f, *i.e.* all x for which f is defined. In this work, the function f is the pressure anomaly distribution along a line in latitudinal or longitudinal direction. For the purpose of data reduction, the function is represented by a linear combination of basis elements P_l. Then only the coefficients α_l associated with the basis elements are kept. In nature, the pressure distribution is smooth in any direction, but contrary to our assumptions above, it is not belonging to a finite dimensional space of functions. Consequently, we can only try to approximate it by a function $f \in X_N$. The

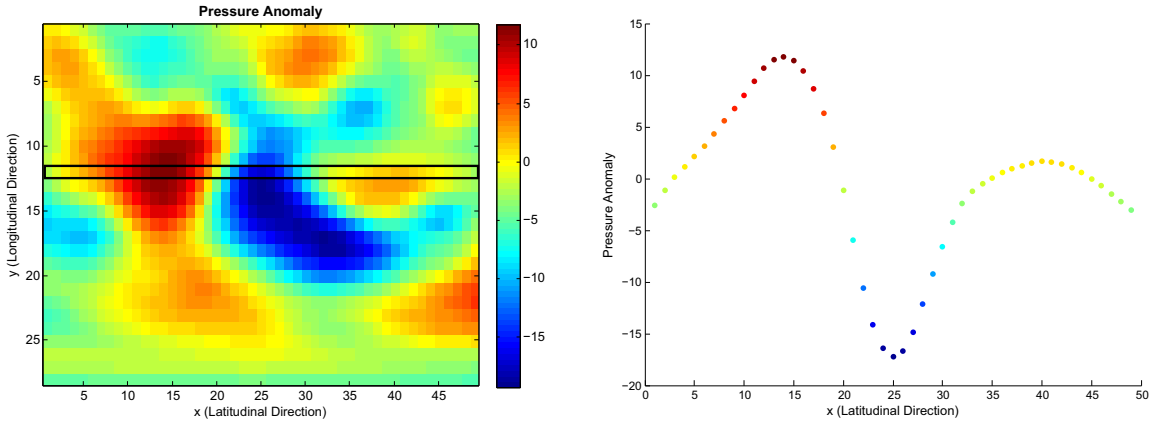

Figure 2.2: Discrete pressure map (left). The rectangle indicates the sample line in latitudinal direction (right), along which the polynomial is fitted.

order of accuracy of such an approximation increases with the number of basis functions N. In the present situation, the given data contains the pressure only at discrete points on a grid. For fitting a function along a row or column of the pressure distribution, Eq. (2.1) has to hold for each of the grid points along that line. This leads to a system of equations from which the coefficients can be computed as follows: Let $Z(t) \in \mathbb{R}^{28\times 49}$ be the discrete pressure distribution at time t and let $Z_{i,j}(t)$ indicate the evaluation of the pressure field at the grid point (x_i, y_j), with $i = 1, \ldots, 28$ and $j = 1, \ldots, 49$. Then we can solve for $\alpha, \beta \in \mathbb{R}^N$

$$\begin{pmatrix} P_1(x_1) & P_2(x_1) & \ldots & P_N(x_1) \\ P_1(x_2) & P_2(x_2) & \ldots & \vdots \\ \vdots & \vdots & \ddots & \vdots \\ P_1(x_{49}) & \ldots & \ldots & P_N(x_{49}) \end{pmatrix} \begin{pmatrix} \alpha_1^i(t) \\ \alpha_2^i(t) \\ \vdots \\ \alpha_N^i(t) \end{pmatrix} = \begin{pmatrix} Z_{i,1}(t) \\ Z_{i,2}(t) \\ \vdots \\ Z_{i,49}(t) \end{pmatrix}$$

or in shorthand

$$\begin{aligned} \left(P_l(x_k)\right)_{kl} \left(\alpha_l^i\right)_l &= \left(Z_{i,k}\right)_k \\ \iff: \qquad P^h \vec{\alpha}^i &= \vec{Z}^i \end{aligned} \tag{2.2}$$

for fitting a function to each row i. Likewise, we can set up a linear equation system for fitting a function to each column j, namely

$$\begin{aligned} \left(P_l(y_\kappa)\right)_{\kappa l} \left(\beta_l^j\right)_l &= \left(Z_{\kappa,j}\right)_\kappa \\ \iff: \qquad P^v \vec{\beta}^j &= \vec{Z}^j \end{aligned} \tag{2.3}$$

where $k = 1, \ldots, 49$ and $\kappa = 1, \ldots, 28$ denote the number of columns or rows, respectively, and $l = 1, \ldots, N$ denotes the basis polynomials.

Although it is possible to compute the coefficients with Eqs. (2.2) or (2.3), resp., the question of choosing the basis polynomials still remains. As the pressure distribution along a line is continuous, it can be approximated by polynomials. Consequently, the most obvious choice would be the monomial basis $\{1, x, x^2, \ldots\}$, i.e. $P_l(x) = x^{l-1},\ l \in \mathbb{N}$. The resulting matrix would be the so called Vandermonde matrix. However, it is not suitable for numerical purposes due to its very bad condition number. Choosing Legendre polynomials as a basis avoids those difficulties. Legendre polynomials can be obtained by orthonormalization of the monomial basis on the interval $[-1, 1]$, subject to the condition that $P_l(1) = 1$ (cf. Fig. 2.3). We obtain:

$$\begin{aligned} L_1(x) &= 1, \\ L_2(x) &= x, \\ L_3(x) &= \frac{1}{2}\left(3x^2 - 1\right), \\ &\vdots \\ L_{N-1}(x) &= \frac{1}{2^N N!}\frac{d^N}{dx^N}\left[(x^2-1)^N\right]. \end{aligned}$$

The Legendre polynomials are orthonormal only on the interval $[-1, 1]$. Thus the grid is implicitly assumed to be transformed on $[-1, 1]^2$. For data reduction purposes the number of basis elements has to be chosen much smaller than the number of grid points. Thus (2.2) and (2.3) are overdetermined systems of equations and there does not exist an exact solution. This means that the linear combination of basis elements cannot represent the discrete pressure distribution exactly. However, we want the function to fit with an error as small as possible. The resulting coefficients can be obtained by solving (2.2) and (2.3) by linear regression:

$$\begin{aligned} (L^h)^T L^h \vec{\alpha}^i &= (L^h)^T \vec{Z}^i \\ (L^v)^T L^v \vec{\beta}^j &= (L^v)^T \vec{Z}^j \end{aligned}$$

Here the matrices L^h, L^v denote the analogues to the matrices P^h, P^v in Eq. (2.2) or (2.3), where the polynomials used for the entries are the Legendre polynomials specified

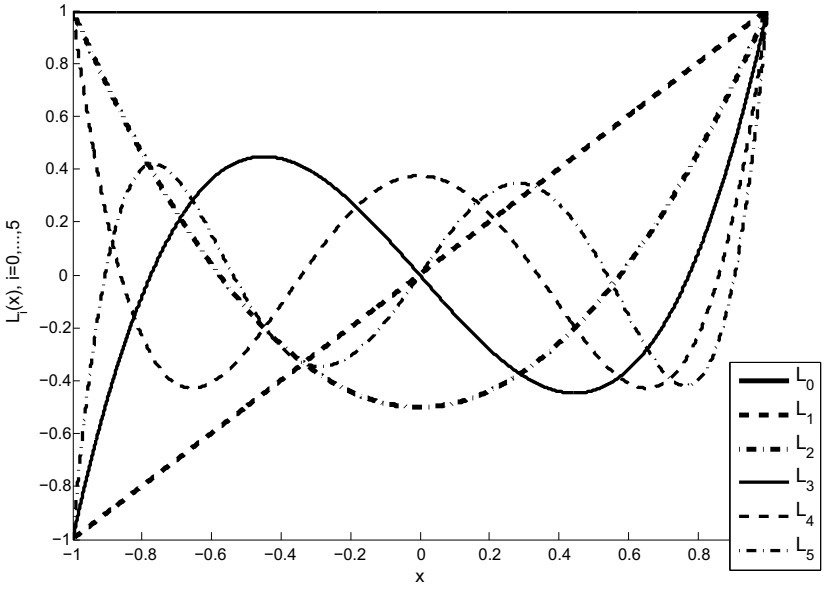

Figure 2.3: Legendre basis polynomials up to fifth order.

before. In order to classify a given pattern with less data, we then collect all coefficient vectors of the pattern:

$$C = \{\vec{\alpha}^1, \ldots, \vec{\alpha}^{28}, \vec{\beta}^1, \ldots, \vec{\beta}^{49}\} \tag{2.4}$$

For a further reduction of data, a function was fitted only to each second row and column of the discrete pressure field. Moreover, the coefficients belonging to the first two Legendre polynomials were neglected. This implies that neither the bias nor the tilt of the pressure distribution are taken into consideration. The reasoning behind this is that a pattern of pressure anomaly is to a greater extent defined by its spatial oscillations than by its offset or slope.

Two-dimensional polynomials

A further reduction based on polynomials can be established by fitting a two-dimensional polynomial. Eqn. (2.1) is extended to:

$$f(x,y) = \sum_{l=0}^{N} \sum_{m=0}^{N-l} \alpha_{lm} P_{lm}(x,y) \qquad \forall x, y \in \mathrm{Dom}(f) \tag{2.5}$$

In this approach the function f is the pressure anomaly distribution of the surface in which x represents the longitudinal direction and y the latitudinal direction. Following

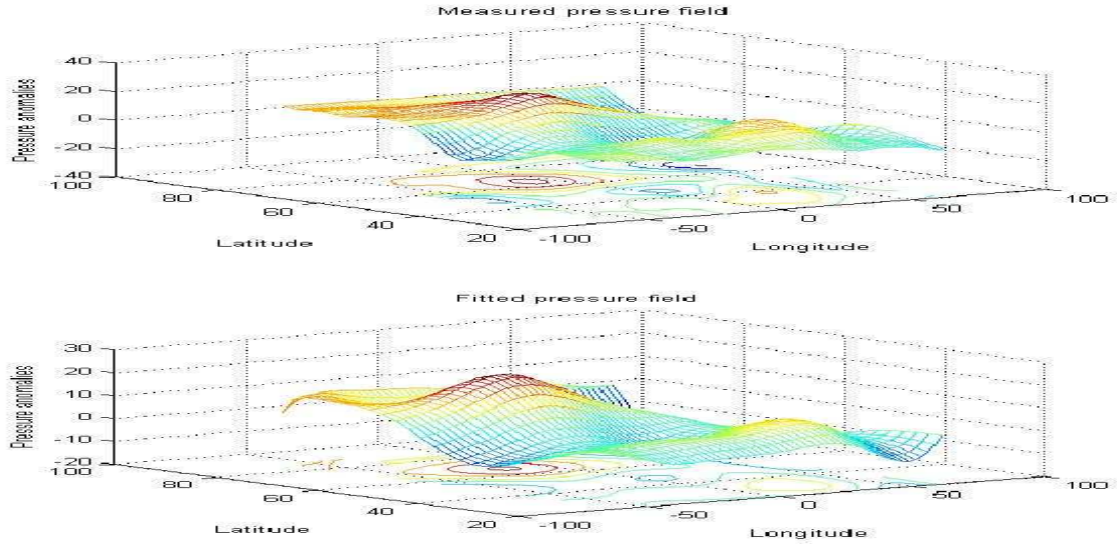

Figure 2.4: Pressure field approximation with an ninth order two-dimensional polynomial function

section 2.2.1 orthonormalization on the domain [-1,1] for both x and y is strongly preferred. However, because of the restricted amount of time only the monomial basis, *i.e.* $\{1, x, y, x^2, xy, y^2, x^3, \dots\}$ was implemented. In analogy to eqns. (2.3) and (2.2) we can set up the system:

$$\begin{pmatrix} P_{00}(x_1,y_1) & P_{01}(x_1,y_1) & \dots & P_{0N}(x_1,y_1) & P_{10}(x_1,y_1) & \dots & P_{N0}(x_1,y_1) \\ P_{00}(x_2,y_1) & P_{01}(x_2,y_1) & & & & & \vdots \\ \vdots & \vdots & \ddots & & & & \vdots \\ P_{00}(x_{49},y_1) & P_{01}(x_{49},y_1) & & \ddots & & & \vdots \\ P_{00}(x_2,y_2) & P_{01}(x_2,y_2) & & & \ddots & & \vdots \\ \vdots & & \ddots & & & \ddots & \vdots \\ P_{00}(x_{49},y_{28}) & P_{01}(x_{49},y_{28}) & \dots & P_{0N}(x_{49},y_{28}) & P_{10}(x_{49},y_{28}) & \dots & P_{N0}(x_{49},y_{28}) \end{pmatrix} \begin{pmatrix} \alpha_{00}(t) \\ \alpha_{01}(t) \\ \vdots \\ \alpha_{0N}(t) \\ \alpha_{10}(t) \\ \vdots \\ \alpha_{NN}(t) \end{pmatrix} = \begin{pmatrix} Z_{1,1}(t) \\ Z_{2,1}(t) \\ \vdots \\ Z_{49,1}(t) \\ Z_{1,2}(t) \\ \vdots \\ Z_{49,28}(t) \end{pmatrix}$$

Generally, a seventh order polynomial for the two-dimensional case gives a good reconstruction of the surface. The number of parameters to be estimated are in this case $1 + 2 + 3 + 4 + 5 + 6 + 7 = 28$. Figure 2.4 shows the approximation for a 9th order polynomial function.

Watershedding

Watersheds were first used in topography. The main idea consists of geographical regions that are divided in so-called catchment basins and the division between two regions is

called the watershed line. Suppose a droplet of water falls down on a surface. This droplet would run down to the lowest point of the region. Adding more droplets would immerse the surface to a lake. The lake will continue to fill until this lake start to flood into a neighbor valley. The line where two valleys, the so-called catchment basins, come together are called the watershed line. Apart from topography the watershedding transform is frequently used in image processing. The pressure anomalies considered in this report can also be viewed as a topographic surface. The watershedding approach is used as a tool for data reduction by obtaining areas of high and low anomalies.

Many algorithms exist that are based on the watershedding principle. The Matlab® implementation which is used in this study is based upon the paper by Vincent and Soille [4]. The algorithm consist of two steps: sorting and flooding. Let $Z(t) \in \mathbb{R}^{28\times 49}$ be the discrete pressure distribution at time t and let $Z_{i,j}(t)$ indicate the evaluation of the pressure field at the grid point (x_i, y_j), with $i = 1, \ldots, 28$ and $j = 1, \ldots, 49$. Because it is assumed that high pressure anomalies are equally important as low pressure anomalies, pressure distribution is transformed such that $\tilde{Z}(t) = -|Z(t)|$. In this way, high pressure anomalies are regarded as catchment basins. For each time point the watershed transform is applied to $\tilde{Z}(t)$ and result in the watershed matrix $W(t)$. Further details and an exact description of the algorithm can be found in [4]. An example of a watershed transform is given in figure 2.5. From the watershed transform $W(t)$ information from the catchment basins is extracted such as the center and total area. By selecting the p most important basins, *i.e.* those with the lowest watershed index or in other words with the largest pressure anomaly, the number of variables is reduced dramatically.

2.2.2 Data Processing and Evaluation

Legendre Polynomials

First of all, a temperature threshold T_{ext} is defined above which a temperature shall be regarded as being extreme. Throughout the simulations, the topmost five per cent of temperature observations were regarded as extreme. As mentioned above, the set of patterns associated to an 'extreme' temperature is then arbitrarily divided into two disjoint subsets: one for calibrating and one for validating the model:

$$I = \{t \mid T(t) \geq T_{\text{ext}}\} := I_{\text{cal}} \dot{\cup} I_{\text{val}}.$$

That is to say: the model is set up with the patterns associated to I_{cal}, and with the patterns belonging to I_{val}, the correctness of the results is checked. Subsequently, for a

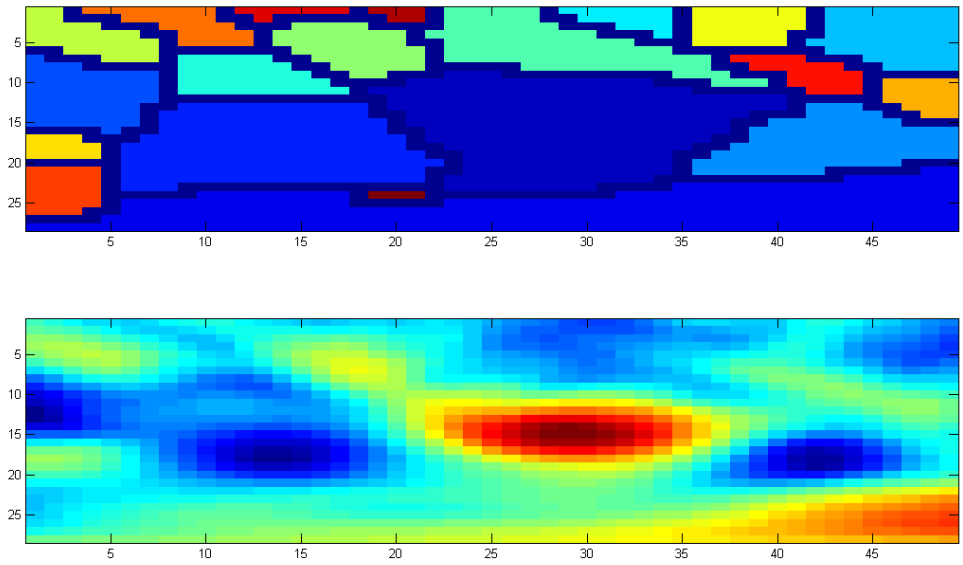

Figure 2.5: A pressure anomaly field and its watershed transform. The x and y axis are the indices are the i and j indices representing the lattitude/longitude of the anomaly field

specific time point t_0 an error $\epsilon(t_0)$ is assigned to each pattern $Z(t_0)$. This error indicates how 'far' that pattern is away from the patterns $\{Z(t) \mid t \in I_{\text{cal}}\}$:

$$\epsilon(t_0) := \min_{t \in I_{\text{cal}}} \|C(t_0) - C(t)\| \tag{2.6}$$

where $C(s)$ denotes the set of characteristic parameters for a pattern $Z(s)$. The error can be measured in any suitable norm, for example the L^2 vector norm.

Two-dimensional polynomials

Although the used data reduction reduction technique is based on the same idea as the Legendre polynomials, a different evaluation technique was performed for the two-dimensional polynomial. Here, the evaluation is based on linear regression.

As in section 2.2.2 the extremes are divided in a calibration and validation subset. In addition, the non-extreme patterns are also divided in a calibration and validation subset. Therefore, the calibration and validation data sets need to contain an equal amount of the interesting extremes compared to the much larger amount of non-extreme data.

$$J = \{t \mid T(t) < T_{\text{ext}}\} := J_{\text{cal}} \dot{\cup} J_{\text{val}}.$$

Hence, the calibration and validation data sets are formulated as:

$$\Gamma_{\text{cal}} = I_{\text{cal}} \cup J_{\text{cal}}$$
$$\Gamma_{\text{val}} = I_{\text{val}} \cup J_{\text{val}}$$

A linear model to predict the local temperature based on the polynomial parameters is proposed:

$$T_{\text{local}}(t) = \alpha(t)\gamma + e(t)$$

with α the time dependent polynomial parameters that define the circulation pattern, γ the model parameters and $e(t)$ the error term. Based on the calibration data set the model parameters γ are estimated by linear regression.

$$\gamma = A^{+}T_{\text{local}}$$

with A^{+} the pseudo-inverse of $[\alpha(t_0), \alpha(t_1), \ldots, \alpha(t_n]^T$. Both calibration and validation data sets are used to estimate the local temperature by:

$$\hat{T}_{\text{local}}(t) = \alpha(t)\hat{\gamma}$$

Watershedding

Before the catchment basins are projected onto local extremes meteorological information must be incorporated. The local extreme is a nonlinear function of the catchment basin and perhaps of the interaction between catchment basins. A first approach was done by constructing a function based on distance, anomaly and area of the catchment basin. Let $\vec{B}_i(t)$ a vector with the variables of catchment basin i at time t extracted from the watershed transform $W(t)$. The local temperature anomaly can be modeled by:

$$T_a(t) = \sum_{i=1}^{p} \delta_i f(\vec{B}_i) + e(t) \tag{2.7}$$

where $f(\vec{B}_i)$ is a nonlinear function with variables from catchment basin i, δ the parameter vector and $e(t)$ the error term. The model is linear in its parameters and, hence, these parameters δ are estimated with an ordinary least squares approach, *i.e.* $\min_\delta ||e(t)||_2 \ \forall t$. Because the system now is largely overdetermined, division into a calibration and validation is not needed. Results are evaluated by comparing the estimated and measured local temperatures of the total data set. Local extremes are part of the data and verification is possible.

2.3 Results

2.3.1 Legendre Polynomials

For testing the L^2-norm comparison method, the set of patterns belonging to an extreme temperature was divided into calibration and validation patterns, analogously to the explanations above. The set of extreme patterns is divided in several fashions:

half: every second pattern is used for calibration, the other half used for testing/validation.

thirds: every third pattern is used for validations, so that 66% of patterns are used for calibration.

rand: each extreme pattern gets assigned a random number from a uniform distribution on the interval [0,1]. For validation, only the patterns with a random number higher than 2/3 are taken.

Concerning the order of the fitted polynomial, an integer value around 4 was chosen. This is sensible, as the pressure distribution along one direction usually contains $n = 2$ to $n = 4$ major high or low pressure areas. As these areas should correspond to the extremes of the fitted polynomial, we need a polynomial degree of $n - 1$. The error was measured in the standard L^2 vector norm. As can be seen from any of the plots in Fig. 2.6, there is no clear visible distinction between the two groups 'errors of non-extreme patterns' (plotted in red) and 'errors of validation patterns' (plotted in green). What can be seen, however, is the (anticipated) tendency of the 'green mean' to be below the 'red mean', i.e. that the patterns belonging to an extreme temperature have on average a lower error than those arbitrary, non-extreme patterns.

Choosing a higher order of polynomial does improve the distinction between the two groups. Nevertheless, taking a too high order of polynomial increases the danger of unnatural oscillatory behavior when fitting the polynomial. Concerning the change of the fashion of partitioning the validation set, the following can be observed: The two groups are the more distinct the more patterns for calibration are used. This is a result one would also expect by common sense.

2.3.2 Two-dimensional polynomial

In figure 2.7 a linear trend is clearly observable. However, it can be clearly seen that the linear trend bends off in the top right corner, just before the crossing horizontal and

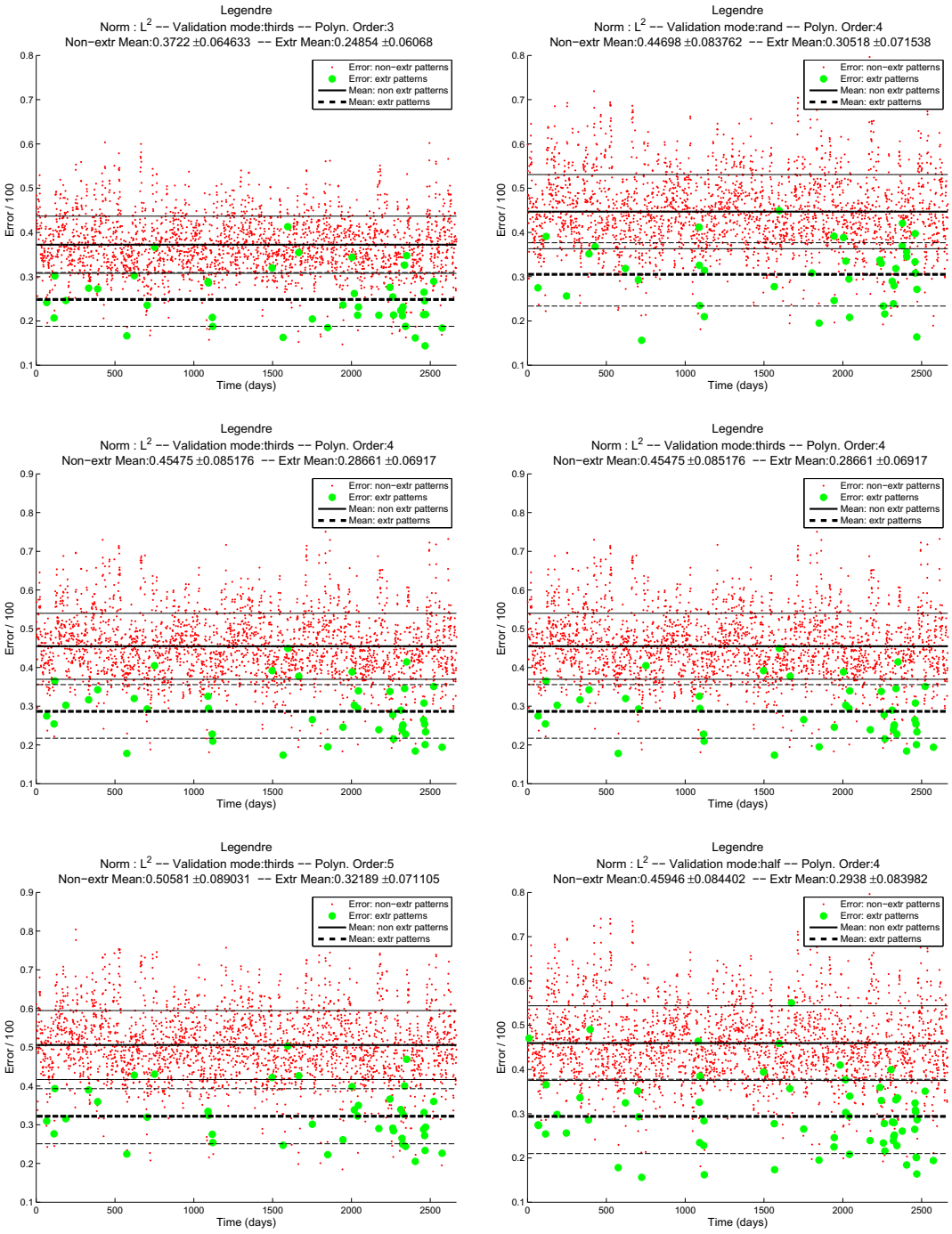

Figure 2.6: Comparison of different polynomial orders (left column – with validation mode `thirds`) and comparison of different validation modes (right column – with polynomial order 4).

vertical lines. These are the lines that distinguish the ordinary values from the extremes. This is exactly the part in which we are interested. When we look at the histogram (see

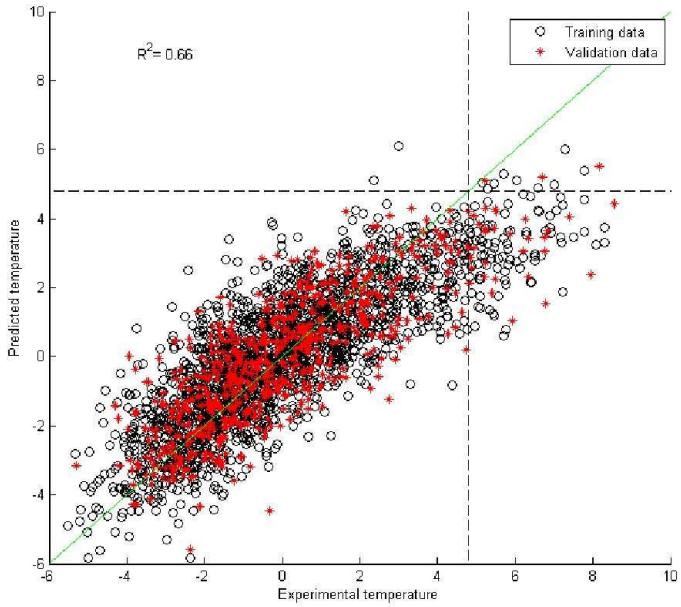

Figure 2.7: Measured vs. Predicted temperature anomalies from the 2-dimensional polynomial with 'o' calibration data and '*' validation data

figure 2.8 of how the local temperatures are distributed) it is clear that it is right tailed. In this tail the extremes are defined. Unfortunately, this tail seems hard to predict. Several procedures have been tried to improve the results, such as a log-transformation of the local temperatures and a neural network approach to account for nonlinearities. These procedures did not improve the results visibly (results not shown).

2.3.3 Watershedding

In this specific example five watersheds are taken for each circulation pattern. The function $f(B)$ from eqn. (2.7) is given by:

$$f(B_i) = \frac{\sin(\alpha) \cdot P \cdot A}{dist} + \frac{\cos\alpha \cdot P \cdot A}{dist}$$

with α the angle between the location of the local measurement and the location of the center of the watershed; $dist$ the distance between the center of the watershed and the local measurement; P the maximum pressure anomaly in the watershed; and A the total area of the watershed. In figure 2.9 a slight linear trend is visible but it is clearly not sufficient. Local extremes cannot be predicted in the current framework.

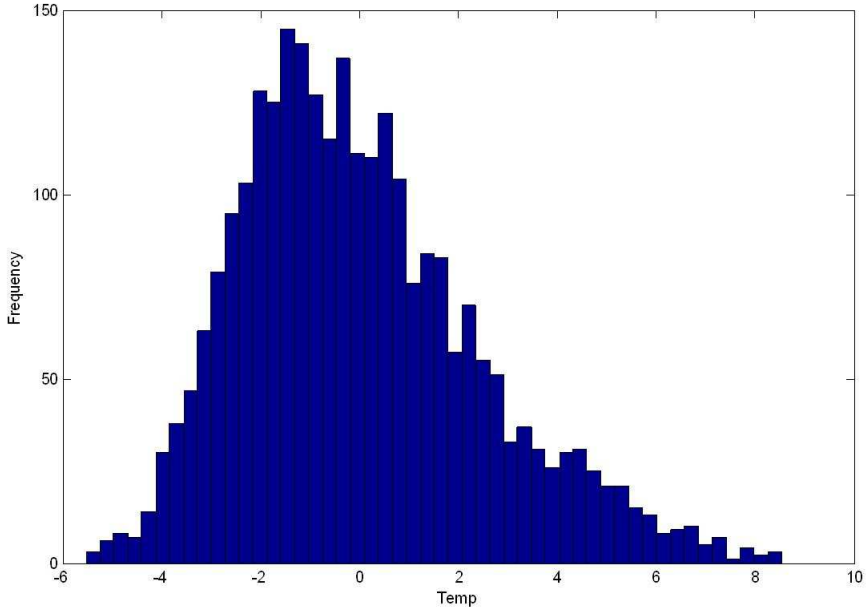

Figure 2.8: Histogram of the measured local temperature anomalies

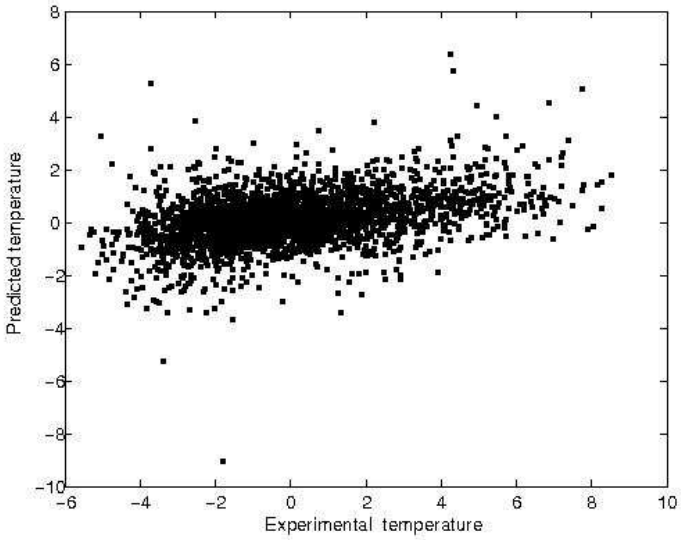

Figure 2.9: Measured vs. Predicted temperature anomalies from the watershed transform

2.4 Discussion

In the Legendre polynomial the groups of 'errors of non-extreme patterns' and 'errors of validation patterns' are not clearly distinctive, but we can observe the tendency that the error-mean of the patterns belonging to the validation set is less than the error-mean of the patterns belonging to the set of non-extremes. Consequently, the method of L^2-norm comparison can only state whether a (new) pattern is similar to a pattern for which an extreme temperature has been recorded. Our tests show that it is not possible to state from just the L^2-error of that pattern whether there will be an extreme temperature or not. The method of comparing the norms can only give a tendency, but not lead to a decision.

Although the evaluation method differed a similar statement can be made about the 2-dimensional polynomial approach. A linear trend is clearly visible in figure 2.7. Only twelve out of 133 extremes (from the total data set), however, are predicted as extremes which is less then 10%. A decision cannot be given based on this relationship.

These results indicate that the local temperature is determined by more than just the pressure distribution on that particular day. A suggestion for further work might be to take other factors into account like moisture or cloudiness. An initial idea that has not been worked out is to use the dynamic changes of the patterns, *i.e.* subtracting pressure fields of two successive days.

The watershed procedure showed poor results. The possibilities of using the basins, however, are very large. In the presented approach only the basins with the largest absolute anomaly were taken into account. Improvements are likely when additional information is included. For instance, it is likely that the pressure anomaly above the local temperature is an important feature. Furthermore, interactions between pressure systems may be good predictors for local extremes. In conclusion, the watershed approach is interesting because of its simplicity and by retaining physical interpretability. Due to this physical interpretability expert knowledge is required to implement a sensible relationship from the basins to the local temperature.

2.5 Concluding remarks

Three methods for data reduction have been presented in order to predict local extremes from large scale circulation patterns. Although the results show trends that relate prediction of local extremes with measurements, these trends are not sufficient to reliably predict typical circulation patterns that cause local extremes. The methods, though, were not fully explored in this report. Further development of the methods with contribution

of export knowledge of the application area is needed to improve the results.

Bibliography

[1] Michelangeli, P. A., Vautard, R., and Legras, B. (1995). Weather regimes - recurrence and quasi stationarity. *Journal of the Atmospheric Sciences*, 52(8):1237–1256. ISI Document Delivery No.: QV955 Times Cited: 105 Cited Reference Count: 30.

[2] Panja, D. and Selten, F. M. (2007). Extreme associated functions: optimally linking local extremes to large-scale atmospheric circulation structures. *Atmospheric Chemistry and Physics Discussions*, 7(5):14433–14460.

[3] Salameh, T. and Dobrinski, P. (2008). Extreme climatic events and north atlantic weather regimes: uncertainty assessment using era-40 and ncep re-analyses. *Geophysical Research Abstracts*, 10:EGU2008–A–8266.

[4] Vincent, L. and Soille, P. (1991). Watersheds in digital spaces: an efficient algorithm based on immersion simulations. *Pattern Analysis and Machine Intelligence, IEEE Transactions on*, 13(6):583–598.